

THE INFLUENCE OF TROPICAL NORTH ATLANTIC SST ON PRECIPITATION IN THE
PERUVIAN AMAZON OVER THE PAST ~1500 YEARS

by

Sarah R. White

A Prepublication Manuscript Submitted to the Faculty of the

DEPARTMENT OF GEOSCIENCES

In Partial Fulfillment of the Requirements
for the Degree of

MASTER OF SCIENCE

In the Graduate College
THE UNIVERSITY OF ARIZONA

2011

The influence of tropical North Atlantic SST on precipitation in the Peruvian Amazon over the past ~1500 years

Sarah White¹, Jonathan Overpeck^{1,2}, Mark Bush³, Scott Saleska⁴

¹Department of Geosciences, University of Arizona

²Institute of the Environment, University of Arizona

³Department of Biological Sciences, Florida Institute of Technology

⁴Department of Ecology and Evolutionary Biology, University of Arizona

Abstract

The effects of rising greenhouse gas concentrations on precipitation and vegetation in the Amazon Basin is a topic of significant interest for both the public and scientific communities. Under future climate change the Amazon region is projected to warm several degrees by 2100, but model projections of precipitation change remain uncertain. Without reliable projections of future precipitation, it will be difficult to estimate how vegetation will be impacted by climate change. To help understand the full range of natural hydroclimatic variability in the Peruvian Amazon, as well as the large-scale controls on this variability, we produced a multi-centennial multi-indicator record of hydroclimatic variability for the region using sediments from a small lake. Employing both elemental abundances inferred from scanning micro-X-ray fluorescence (μ -XRF) techniques, and grain size measurements, we show that the full range of regional hydroclimatic variability includes regular (i.e., about one per century in the last ca. 1500 years) droughts. Furthermore, our results suggest that tropical North Atlantic sea surface temperature (SST) variability has been the main influence driving changes in precipitation on decadal to centennial timescales, with warmer SSTs associated with reduced precipitation over the Amazon region. A warmer North Atlantic Ocean (NATL) displaces the Intertropical Convergence Zone (ITCZ) further north, leading to convergence north of the equator and subsidence over the

Amazon. The opposite occurs when the NATL is anomalously cool. Eastern Tropical Pacific SST variability may have also played a lesser, but still important role on climate in this region. Continued warming of surface air temperatures in the Amazon and SSTs in the tropical NATL could favor more severe drought in the western Amazon Basin in the future, but in any case, severe drought should be considered a real threat for the region until proven otherwise.

Introduction

The Amazon Basin is consistently an area of interest when discussing future climate change, as the full effects of increasing greenhouse gas emissions in this region are still unknown, but are potentially significant for the carbon cycle, biodiversity, and regional populations. Temperature is expected to rise 2-4°C over the 21st century, but precipitation projections are not as well constrained, especially for the western Amazon, with some models showing an increase in the frequency and severity of drought events, and others showing an increase in precipitation or no change at all [*Christensen et al.*, 2007; *Malhi et al.*, 2008; *Betts et al.*, 2004, 2008]. Recent studies seek to determine the effects of these future changes on Amazonian vegetation by studying recent droughts and the resultant vegetation changes [*Saleska et al.*, 2007; *Lewis et al.*, 2011; *Phillips et al.*, 2009]. The potential conversion of forest to savannah has large implications for both the carbon cycle and biodiversity in this biologically diverse region [*Betts et al.*, 2004, 2008]. However, without accurate predictions of future precipitation, it is difficult to forecast just how vegetation will change in the future. In addition, it is critical to know the full range of climate variability that the Amazon ecosystems have endured prior to the rise of anthropogenic climate change.

Tropical SST, both in the Eastern Pacific and NATL oceans, affects rainfall over the Amazon Basin and has been shown to cause extreme drought in this region, with warm SST resulting in reduced precipitation (when the NATL is warm, the ITCZ is displaced northward leading to convergence north of the equator, and subsidence over the Amazon) [Yoon and Zeng, 2010; Grimm and Zilli, 2009; Li et al. 2006; Harris et al., 2008, Lewis et al., 2011]. The future effects of increasing Pacific SST on the El Niño/Southern Oscillation (ENSO) are still debated, and increasing Atlantic SST would likely result in drought in the Amazon [Meehl et al., 2007; Yoon and Zeng, 2010]. In order to understand how climate change-induced SST increases might affect precipitation in the future, we must first understand how tropical SSTs have influenced rainfall in the past.

Paleoclimate studies have proven useful in the search to understand tropical Pacific and Atlantic SST variability, as well as long-term climate variability over the Amazon Basin, on decadal and longer time scales. Reuter et al. [2009] used oxygen isotopes from a Peruvian speleothem to show that prior to the 20th century, rainfall in northern South America was correlated with tropical Atlantic SST variability. However, this relationship breaks down in the 20th century, which they attributed to a strengthened ENSO influence. Past Pacific SST variability has similarly been inferred from regional climate changes recorded in oxygen isotopes from multiple ice cores in Peru and Bolivia [Thompson et al., 1984; Bradley et al., 2003; Henderson et al., 1999]. Also using ice core oxygen isotope records, Thompson et al. [1995] demonstrated that strong warming dominated the Amazon over the last two centuries. Unfortunately, the interpretation of oxygen isotope variations found from tropical ice cores is only recently beginning to be understood [Hoffmann, 2003; Vuille and Werner, 2005]. Other records from this region that record past climate variability have been collected from Lake

Titicaca, located on the Altiplano, and the Cariaco Basin located offshore of Venezuela [*Baker et al.*, 2001; *Haug et al.*, 2001; *Black et al.*, 2007]. However, reconstructions from Lake Titicaca are low-resolution, and Cariaco Basin proxy records are more influenced by climate variability in northern South America rather than the Amazon Basin. Thus, high-resolution records from the Amazon Basin itself are needed.

Here we use lake sediments from north-central Peru, on the western edge of the Amazon Basin at 600m elevation, to reconstruct precipitation over the past ~1500 years. We show that rainfall over this period appears to be strongly linked to tropical NATL SST on decadal to centennial timescales. Tropical Pacific SST appears to have also played a smaller, but still important, role in driving climate in this region. It also appears that the western Amazon has been affected by multiple droughts over pre-industrial time.

Study Site

Lake Limón (6°43'S, 76°14'W) is located in north-central Peru at the base of the eastern flank of the Andes Mountains (Fig. 1). It lies at 600m in elevation on the western edge of the Amazon Basin and is a relatively small, crescent-shaped basin (~535m in length and ~80m in width). The lake has one small, hypersaline inlet and one outlet, and at its maximum depth of 13.6m it reaches salinity levels of 70‰. The lake is located within a salt dome, and thus the hypersalinity is most likely due to natural seepage of NaCl. Mineral composition of the sediment is mostly quartz, but also contains calcite and muscovite. Lake Limón is anoxic below ~5m, inhibiting bioturbation and favoring the preservation of local climate signals.

Mean monthly temperatures near Lake Limón exhibit a limited annual range of ~2°C, and annual precipitation has a bimodal distribution that closely follows the seasonal migration of the

ITCZ and the South American Monsoon System (SAMS) (Fig. 1) [Correa-Metrio et al., 2010]. Precipitation is highest during austral spring, in September and October, when surface heating is strongest over northern Peru. This corresponds to the onset of the wet season over South America and the start of the SAMS. The region of highest precipitation then migrates southeast to the subtropics, where it remains for the duration of the summer, reducing precipitation over northwestern South America. In austral fall, precipitation over Lake Limón is again high as the ITCZ migrates back into the northern hemisphere and the SAMS decays, passing over northern Peru [Vera et al., 2006; Zhou and Lau, 1998, 2001].

Eastern tropical Pacific and Atlantic SST play a major role in driving precipitation on interannual to decadal time scales over the Amazon through their influence on the location of the ITCZ and the trade winds (Fig. 2). Warm tropical NATL SST results in reduced precipitation over the Amazon. The warmer waters north of the equator displace the ITCZ northward leading to convergence north of the equator and subsidence over the Amazon region. Conversely, when tropical NATL SSTs are anomalously cool, the ITCZ is shifted southward, resulting in enhanced moisture over Amazonia. Precipitation over most of the Amazon reacts similarly to changes in eastern tropical Pacific SST, particularly during ENSO events. During an El Niño event, rainfall is typically reduced over the Amazon as a whole, and conversely, precipitation is typically enhanced during a La Niña event [Marengo and Hastenrath, 1993; Yoon and Zeng, 2010; Grimm and Zilli, 2009; Paegle and Mo, 2002]. However, our lake location, at the base of the Andes Mountains on the very western edge of the Amazon, responds to tropical ENSO in a slightly different manner than the rest of the Amazon Basin. El Niño events have been shown to result in slightly higher annual precipitation near Lake Limón, with La Niña events resulting in slightly

lower annual precipitation. However, during La Niña events, there is anomalously high rainfall during the month of May [*Correa-Metrio et al.*, 2010].

Methods

Field Methods:

We retrieved 3 piston cores (LP-1, LP-2, and LP-3), 4-5m in length, from multiple drives near the center of Lake Limón at a water depth of 13m. We also retrieved 6 gravity cores (LU-1, LU-2, LU-3, LU-4, LU-5, and LU-6), taken from within 50m of the piston cores, in order to capture the sediment-water interface. Each core was taken from between 12 and 13.5m depth and captured the mud-water interface with minimal mixing. We extruded the top portion of each core at 0.25cm increments in order to prevent mixing during transport. For this study, we produced a composite of LP-3 (4.8m long) and LU-5 (1.2m long taken at 12.2m depth) by correlating the two cores where they overlap using both lithologic and chemical tie points.

Age Model:

To construct an age model, 21 radiocarbon dates were obtained from terrestrial material found in both gravity and piston cores, and 12 ^{210}Pb measurements were acquired from the uppermost sediment in the gravity core (Table 1). We correlated the cores and built a master chronology using both lithologic and chemical tie points. To determine if there is a reservoir effect in the lake, we sampled modern unsubmerged terrestrial vegetation and modern submerged aquatic macrophyte samples for ^{14}C . Both samples reflected the presence of bomb-produced radiocarbon, and the fraction modern carbon ($F^{14}\text{C}$) values fall within error of each other (1.016 ± 0.012 , 1.033 ± 0.011 , respectively) [*Hua and Barbetti*, 2004; *McCormac et al.*,

2004]. We therefore determined that there is no reservoir effect in this lake. We excluded three ^{14}C dates because there was too little carbon to obtain an accurate date. We also excluded two dates taken on leaves that resulted in outliers implying the leaves were most likely washed in years after deposition on the catchment floor.

Pretreatment for radiocarbon samples was performed using the standard acid-base-acid procedure of HCl and NaOH to remove any carbonates and humic acids [Hedges *et al.*, 1989]. The samples were then combusted at the University of Arizona Accelerator Mass Spectrometry (AMS) facility. Twelve additional samples, taken at 2cm intervals from the top of the gravity core (including extruded sediment), were sent to The Florida Institute of Paleoenvironmental Research (FLIPER) laboratory at The University of Florida for ^{210}Pb and ^{137}Cs activity measurement. ^{210}Pb ages were calculated using the constant rate of supply model [Appleby and Oldfield, 1983; Appleby, 2001]. Measured ^{137}Cs values were extremely low and were thus not included in the age model.

The age model was constructed using a non-Bayesian, ‘classical’ age-depth model program known as *clam* [Blaauw, 2010]. This software first calibrates ^{14}C dates using the SHCal04 calibration dataset, then produces a “best fit” age model using a LOESS smooth curve function through both ^{210}Pb and ^{14}C dates [McCormac *et al.*, 2004]. After all age reversals were removed, over 1000 iterations remained to produce the final age model (Fig. 3).

μ -XRF and Grain Size Procedures:

To sample the sediment for μ -XRF analysis, we took thin-sections from both gravity and piston cores. We then performed acetone exchanges to remove water in the sediment. In order to reduce noise due to water formation and surface roughness during μ -XRF measurements, we

embedded the sediment in resin using standard procedures as described in *Pike and Kemp* [1996]. We measured the elemental abundances of 11 elements (Al, Si, S, Cl, K, Ca, Ti, Mn, Fe, Rb, and Sr) using an EDAX Eagle III tabletop scanning μ -XRF analyzer at the University of Arizona. Machine specifics can be found in *Shanahan et al.* [2008].

Grain size samples were taken from the gravity core (including surface sediment extruded in the field) at contiguous 0.5cm intervals and pretreated using a modified technique from D. Rodbell (<http://www1.union.edu/rodbelld/grainsizeprep.htm>). To extract any carbonates we added a 15% HCl solution. H_2O_2 is the standard protocol for removing any organic material, however, to save time we first treated the samples for 3 days with bleach (6% NaClO) which has also been shown to remove organics [*Gaffey and Bronnimann*, 1993]. We then used a 30% H_2O_2 solution to remove any remaining organics. Finally, we used a 1M NaOH solution to remove any biogenic silica, and added a dispersant $(NaPO_3)_6$ to prevent aggregation of clay-sized particles. Between each step we rinsed, centrifuged, and decanted all samples three times. Samples were then measured using a University of Arizona Malvern Mastersizer 2000 laser-diffraction particle size analyzer together with a Hydro 2000S sample dispersion accessory. We measured each sample 5 times at 3500 rpm and 50% sonication for 1 minute prior to and during measurement, and then averaged the results.

Results and Discussion

We used both elemental abundances and grain size to determine hydroclimate variability at Lake Limón (Fig. 4). Elemental abundances can trace changes in lake levels, transport energy, and water chemistry within the lake [e.g., *Shanahan et al.*, 2008; *Niemann et al.*, 2009; *Böning et al.*, 2007; *Moreno et al.*, 2007]. The profiles of all elements are shown in Appendix A. To

determine which elements explain the majority of the variability, we performed principal components analysis (PCA) on the annualized elemental correlation matrix. The first 3 principal components together explain 79.3% of the variance, but only the first two exhibit correlations with climate and are discussed here. The first principal component explains 38% of the variance and is positively correlated with the abundance of the terrestrial elements Al, K, Ti, Fe and Rb, and negatively correlated with Ca abundance. Thus, positive values indicate more terrestrial elements and less Ca, and negative values indicate more Ca and less terrestrial elements. The second principal component explains 24% of the variance and is positively correlated with Si, and inversely correlated with S, Ca, Mn, Fe, and Sr abundances. The loadings of each element on the first 3 PCs are shown in Appendix B. Both principal components vary significantly on decadal and centennial timescales, but also include periods of interannual extremes as well.

We also use grain size as an independent indicator of Lake Limón's hydroclimatic variability. Changes in grain size can indicate changes in transport energy and lake level within the watershed. Thus, we attempted to provide an independent test of our interpretation of the XRF data by sampling the surface core (LU-5) for grain size. Clay size particles ($<3.9\mu\text{m}$) were absent throughout the sampled period and are therefore not shown. Nearly all of the particles are silt sized ($3.9\text{-}62.5\mu\text{m}$) for the majority of the core. However there are four periods in which the percentage of sand sized ($>62.5\mu\text{m}$) particles increases to at least 20%, and at times as much as 50%.

Terrestrial elements, such as those driving PC1, can indicate lower lake level (through an increase in the amount of erodible material due to increased catchment size), or increased transport (via runoff). CaCO_3 normally precipitates under drier conditions, and since it drives PC1 in the opposite direction as the terrestrial elements, this would indicate that PC1 is recording

increased transport as opposed to lower lake level [Cohen, 2003]. We thus interpret this signal to be related to precipitation. Normally we would use instrumental records of precipitation to confirm this hypothesis. However, precipitation records from this region are sparse and only overlap with elemental data for at most 20 years; and although our proxy data are relatively high-resolution, they are not annual. Fortunately, *Yoon and Zeng* [2010], among others, have shown that both the tropical Pacific and NATL oceans play a major role in precipitation over this region [Grimm and Zilli, 2009; Paegle and Mo, 2002]. When we compare PC1 to SST data (NCDC v3b ERSST reconstruction obtained from the KMNI Climate Explorer) over the instrumental period, we find that it correlates significantly with the core NATL source region (6-22°N and 80-15°W) described by *Yoon and Zeng* [2010] ($r = -0.63$, $p < 0.05$; Table 2; Fig. 5). This supports our interpretation that PC1 reflects precipitation, and shows that it is controlled, at least in part, by tropical NATL SST, with warm SST resulting in less precipitation and cool SST resulting in more precipitation.

Based on the modern NATL-Amazon teleconnection pattern and the relationship between PC1 and tropical NATL SST, we use our 1500 year record of elemental abundance to infer past precipitation anomalies. We identify positive rainfall anomalies from 564 to ~570 AD, ~650 to 700 AD, and ~1280 to 1365 AD, as well as multiple periods in which precipitation is well below average, such as ~700 to 750 AD, ~925 AD, and ~1640 to 1660 AD. There is also a shift from wetter to drier conditions starting at ~1350 AD. Grain size also shows a shift from coarser to finer grains around the same time that PC1 shows a shift to drier conditions, implying that precipitation is in fact decreasing during this time. However, % sand increases again at ~1735 AD and during the 20th century, which is not recorded in PC1. This may be explained by the fact that during grain size pre-treatment we removed any biogenic Si and CaCO₃ from the samples.

However, both of these signals are still contained in the XRF record. In addition, since the lake is strongly stratified, the changes in grain size may also be impacted by density currents. Therefore, it may prove difficult to infer much from a comparison of our grain size record with the XRF record.

Our record shows variable and unexpected correlations with paleoclimate records from other sites in tropical South America. The %Ti record of runoff to Cariaco Basin follows a similar pattern to PC1 on multi-decadal timescales with a 15-year bin correlation of 0.5 ($p < 0.01$; Table 2; Fig. 6) [Haug *et al.*, 2001]. However, we would expect these sites to be negatively correlated based on the interpretation of each record. A possible alternative hypothesis could be that since the Ti input to Cariaco Basin is coming from northern South America, it is responding in a similar manner as PC1 to tropical NATL SST. According to Yoon and Zeng [2010], tropical NATL SST is negatively correlated with precipitation over almost all of South America north of 20°S. Thus, when the NATL is warm, precipitation is reduced over much of the region in which the rivers carrying Ti to Cariaco Basin originate. Conversely, when the NATL is cool, increased precipitation over northern South America would result in increased runoff from the rivers carrying Ti to Cariaco Basin. This relationship is similar to the one between PC1 and tropical NATL SST and could be the explanation for why we see a positive correlation between PC1 and %Ti at Cariaco Basin.

Records of NATL SST also seem to follow PC1 on decadal timescales (Fig. 6). Gray *et al.* [2004] reconstruct NATL (0-70°N) SST anomalies using tree-ring records from regions with climates strongly linked to NATL SST anomalies. They show strong correlations with the observed anomalies, especially on decadal timescales. They reconstruct the AMO (Atlantic Multidecadal Oscillation) by simply using a 10 year running mean of the SST data, and find

strong coherence with observed SST in a band from ~30-65 years. When we perform a 15 year bin correlation analysis between the *Gray et al.* [2004] reconstruction and PC1, we find a correlation of $r = -0.35$ ($p < 0.07$; Table 2; Fig. 6). However, other records, such as precipitation from nearby Cascayunga cave and a Mg/Ca SST reconstruction from Cariaco Basin have much weaker correlations with our record of terrestrial elements (Table 2; Fig. 6) [*Reuter et al.*, 2009; *Black et al.*, 2007]. This suggests that the tropical NATL may not be the only influence on precipitation at Lake Limón, and most likely these records as well.

In fact, it appears as though ENSO may also play a small role in climate at Lake Limón. Since PC2 is driven negatively by Fe, Mn, and S, we thus interpret this to be a redox signal as these elements are known to be associated with redox reactions that occur within the water column [*Cohen*, 2003]. Over the instrumental period, PC2 correlates with the Niño3.4 region (Table 2; Fig. 5). This implies that warmer equatorial Pacific SST results in fewer redox elements since PC2 is negatively driven by these elements. In addition, S alone correlates even more strongly with Niño3.4, with an r-value of -0.57. These results imply that ENSO plays an additional role in climate at Lake Limón through the altering of redox reactions within the lake itself.

Conclusions

We present a high-resolution, multi-centennial record of hydroclimate from the central Peruvian region of the Amazon Basin using lake sediment μ -XRF and grain size analyses. We find that the first principal component of the XRF data, which explains 38% of the variance, is positively correlated with multiple terrestrial elements, and negatively correlated with Ca. We thus interpret this signal to be related to precipitation. Based on correlations with tropical NATL

SST instrumental data and reconstructions we find that precipitation is largely influenced by tropical NATL SST. When there are warm conditions in the tropical NATL, the ITCZ is shifted northward, and less precipitation reaches the western Amazon. We also find that the tropical equatorial Pacific may play a smaller, but significant role in the climate of this region through the varying of redox reactions within the lake. With NATL SST projected to increase in the future due to rising greenhouse gas emissions, and the uncertainty with regards to the effects on the ENSO system, it is likely that the western Amazon Basin could see much drier conditions in the future.

Acknowledgments

We thank the NSF Amazon-PIRE program, the Kartchner Caverns scholarship fund, and the Department of Geosciences at the University of Arizona for their funding support. The Paleoecology Lab at the Florida Institute of Technology, and especially Bryan Valencia, were also critical to the success of this research.

References

- Adler, R.F., Huffman, G.J., Chang, A., Ferraro, R., Xie, P., Janowiak, J., Rudolf, B., Schneider, U., Curtis, S., Bolvin, D., Gruber, A., Susskind, J., Arkin, P., 2003. The version 2 global precipitation climatology project (GPCP) monthly precipitation analysis (1979-present). *J. Hydrometeorol* 4, 1147-1167.
- Appleby, P.G., Oldfield, F., 1983. The assessment of ^{210}Pb data from sites with varying sediment accumulation rates. *Hydrobiologia* 103, 29-35.
- Appleby, P.G., 2001. Chronostratigraphic techniques in recent sediments, in *Tracking Environmental Change Using Lake Sediments: Basin Analysis, Coring, and Chronological Techniques*, edited by W.M. Last and J.P. Smol. Kluwer Academic Publ., 171-203.
- Baker, P.A., Seltzer, G.O., Fritz, S.C., Dunbar, R.B., Grove, M.J., Tapia, P.M., Cross, S.L., Rowe, H.D., Broda, J.P., 2001. The history of South American tropical precipitation for the past 25,000 years. *Science* 291, 640-643.
- Betts, R.A., Cox, P.M., Collins, M., Harris, P.P., Huntingford, C., Jones, C.D., 2004. The role of ecosystem-atmosphere interactions in simulated Amazonian precipitation decrease and forest dieback under global climate warming. *Theoretical and Applied Climatology* 78, 157-175.
- Betts, R.A., Malhi, Y., Roberts, J.T., 2008. The future of the Amazon: new perspectives from climate, ecosystem and social sciences. *Phil. Trans. R. Soc. B* 363, 1729-1735.
- Blaauw, M., 2010. Methods and code for 'classical' age-modelling of radiocarbon sequences. *Quaternary Geochronology* 5, 512-518.
- Black, D.E., Abahazi, M.A., Thunell, R.C., Kaplan, A., Tappa, E.J., Peterson, L.C., 2007. An 8-century tropical Atlantic SST record from the Cariaco Basin: Baseline variability, twentieth-century warming, and Atlantic hurricane frequency. *Paleoceanography* 22 (4), PA4204.

- Böning, P., Bard, E., Rose, J., 2007. Toward direct, micron-scale XRF elemental maps and quantitative profiles of wet marine sediments. *Geochem. Geophys. Geosyst.* 8 (Q05004).
- Bradley, R.S., Vuille, M., Hardy, D., Thompson, L.G., 2003. Low latitude ice cores record Pacific sea surface temperatures. *Geophysical Research Letters* 30 (4), 1174.
- Christensen, J.H., Hewitson, B., Busuioc, A., Chen, A., Gao, X., Held, I., Jones, R., Kolli, R.K., Kwon, W.-T., Laprise, R., Magaña Rueda, V., Mearns, L., Menéndez, C.G., Räisänen, J., Rinke, A., Sarr, A., and Whetton, P., 2007. Regional Climate Projections. In: *Climate Change 2007: The Physical Science Basis. Contribution of Working Group I to the Fourth Assessment Report of the Intergovernmental Panel on Climate Change* [Solomon, S., D. Qin, M. Manning, Z. Chen, M. Marquis, K.B. Averyt, M. Tignor and H.L. Miller (eds.)]. Cambridge University Press, Cambridge, United Kingdom and New York, NY, USA.
- Cohen, A. S. (2003). Paleolimnology: The History and Evolution of Lake Systems, Oxford University Press.
- Correa-Metrio, A., Cabrera, K.R., Bush, M.B., 2010. Quantifying ecological change through discriminant analysis: a paleoecological example from the Peruvian Amazon. *Journal of Vegetation Science* 21, 695-704.
- Enfield, D.B., Mestas, A.M., Mayer, D.A., Cid-Serrano, L., 1999. How ubiquitous is the dipole relationship in tropical Atlantic sea surface temperatures? *Journal of Geophysical Research* 104 (7841-7848).
- Gaffey, S.J., Bronnimann, C.E., 1993. Effects of bleaching on organic and mineral phases in biogenic carbonates. *Journal of Sedimentary Petrology* 63 (4), 752-754.

- Gray, S.T., Graumlich, L.J., Betancourt, J.L., Pederson, G.T., 2004. A tree-ring based reconstruction of the Atlantic Multidecadal Oscillation since 1567 A.D. *Geophysical Research Letters* 31 (L12205).
- Grimm, A.M., Zilli, M.T., 2009. Interannual variability and seasonal evolution of summer monsoon rainfall in South America. *Journal of Climate* 22, 2257-2275.
- Haug, G.H., Hughen, K.A., Sigman, D.M., Peterson, L.C., Röhl, U., 2001. Southward migration of the Intertropical Convergence Zone through the Holocene. *Science* 293, 1304-1308.
- Harris, P.P., Huntingford, C., Cox, P.M., 2008. Amazon Basin climate under global warming: the role of the sea surface temperature. *Phil. Trans. R. Soc. B* 363, 1752-1759.
- Hedges, R.E.M., Law, I.A., Bronk, C.R., Housley, R.A., 1989. The Oxford Accelerator Mass Spectrometry Facility: Technical developments in routine dating. *Archaeometry* 31 (2), 99-113.
- Henderson, K.A., Thompson, L.G., Lin, P.-N., 1999. Recording of El Niño in ice core $\delta^{18}\text{O}$ records from Nevado Huascarán, Peru. *Journal of Geophysical Research* 104 (D24), 31053-31065.
- Hoffmann, G., 2003. Taking the pulse of the tropical water cycle. *Science* 301, 776-777.
- Hua, Q., Barbetti, M., 2004. Review of tropospheric bomb C-14 data for carbon cycle modeling and age calibration purposes. *Radiocarbon* 46 (3), 1273-1298.
- Lewis, S.L., Brando, P.M., Phillips, O.L., van der Heijden, G.M.F., Nepstad, D., 2011. The 2010 Amazon drought. *Science* 331, 554.
- Li, W.H., Fu, R., Dickinson, R.E., 2006. Rainfall and its seasonality over the Amazon in the 21st century as assessed by the coupled models for the IPCC AR4. *Journal of Geophysical Research* 111 (D02111).

- Malhi, Y., Roberts, J.T., Betts, R.A., Killeen, T.J., Li, W., Nobre, C.A., 2008. Climate change, deforestation, and the fate of the Amazon. *Science* 319, 169-172.
- Marengo, J.A., Hastenrath, S., 1993. Case-studies of extreme climatic events in the Amazon Basin. *Journal of Climate* 6 (4), 617-627.
- Mayle, F.E., Burbridge, R., Killeen, T.J., 2000. Millennial-scale dynamics of southern Amazonian rain forests. *Science* 290, 2291-2294.
- McCormac, F.G., Hogg, A.G., Blackwell, P.G., Buck, C.E., Higham, T.F.G., Reimer, P.J., 2004. SHCal04 Southern Hemisphere calibration, 0-11.0 cal kyr BP. *Radiocarbon* 46 (3), 1087-1092.
- Meehl, G.A., Stocker T.F., Collins W.D., Friedlingstein P., Gaye A.T., Gregory J.M., Kitoh A., Knutti R., Murphy J.M., Noda A., Raper S.C.B., Watterson I.G., Weaver A.J. Zhao Z.-C., 2007. Global Climate Projections. In: *Climate Change 2007: The Physical Science Basis. Contribution of Working Group I to the Fourth Assessment Report of the Intergovernmental Panel on Climate Change* [Solomon, S., D. Qin, M. Manning, Z. Chen, M. Marquis, K.B. Averyt, M. Tignor and H.L. Miller (eds.)]. Cambridge University Press, Cambridge, United Kingdom and New York, NY, USA.
- Moreno, A., Giralt, S., Valero-Garces, B., Saez, A., Bao, R., Prego, R., Pueyo, J.J., Gonzalez-Samperiz, P., Taberner, C., 2007. A 14 kyr record of the tropical Andes: The Lago Chungara sequence (18 degrees S, northern Chilean Altiplano). *Quaternary International* 161, 4-21.
- Niemann, H., Haberzettl, T., Behling, H., 2009. Holocene climate variability and vegetation dynamics inferred from the (11700 cal. Yr BP) Laguna Rabadilla de Vaca sediment record, southeastern Ecuadorian Andes. *The Holocene* 19 (2), 307-316.

- Paegle, J.N., Mo, K.C., 2002. Linkages between Summer Rainfall Variability over South America and Sea Surface Temperature Anomalies. *Journal of Climate* 15 (12), 1389-1407.
- Phillips, O.L., Aragão, L.E.O.C., Lewis, S.L., Fisher, J.B., Lloyd, J., López-González, G., Malhi, Y., Monteagudo, A., Peacock, J., Quesada, C.A., van der Heijden, G., Almeida, S., Amaral, I., Arroyo, L., Aymard, G., Baker, T.R., Bánki, O., Blanc, L., Bonal, D., Brando, P., Chave, J., de Oliveira, A.C.A., Cardozo, N.D., Czimczik, C.I., Feldpausch, T.R., Freitas, M.A., Gloor, E., Higuchi, N., Jiménez, E., Lloyd, G., Meir, P., Mendoza, C., Morel, A., Neill, D.A., Nepstad, D., Patiño, S., Peñuela, M.C., Prieto, A., Ramírez, F., Schwarz, M., Silva, J., Silveira, M., Thomas, A.S., ter Steege, H., Stropp, J., Vásquez, R., Zelazowski, P., Dávila, E.A., Andelman, S., Andrade, A., Chao, K.J., Erwin, T., Di Fiore, A., Honorio C., E., Keeling, H., Killeen, T.J., Laurance, W.F., Cruz, A.P., Pitman, N.C.A., Vargas, P.N., Ramírez-Angulo, H., Rudas, A., Salamão, R., Silva, N., Terborgh, J., Torres-Lezama, A., 2009. Drought Sensitivity of the Amazon Rainforest. *Science* 323, 1344-1347.
- Pike, J., Kemp, A.E.S., 1996. Preparation and analysis techniques for studies of laminated sediments, in *Palaeoclimatology and Palaeoceanography From Laminated Sediments*, edited by A. E. S. Kemp. *Geol. Soc. Spec. Publ.*, 116, 37-48.
- Reuter, J., Stott, L., Khider, D., Sinha, A., Cheng, H., Edwards, R.L., 2009. A new perspective on the hydroclimate variability in northern South America during the Little Ice Age. *Geophysical Research Letters* 36 (L21706).
- Saleska, S.R., Didan, K., Huete, A.R., da Rocha, H.R., 2007. Amazon forests green-up during 2005 drought. *Science* 318, 612.

- Shanahan, T.M., Overpeck, J.T., Hubeny, J.B., King, J., Hu, F.S., Hughen, K., Miller, G., Black, J., 2008. Scanning micro-X-ray fluorescence elemental mapping: A new tool for the study of laminated sediment records. *Geochemistry Geophysics Geosystems* 9 (Q02016).
- Thompson, L.G., Mosley-Thompson, E., Arno, B.M., 1984. El Niño-Southern Oscillation events recorded in the stratigraphy of the tropical Quelccaya Ice Cap, Peru. *Science* 226 (4670), 50-53.
- Thompson, L.G., Mosley-Thompson, E., Davis, M.E., Lin, P.N., Henderson, K.A., Coledai, J., Bolzan, J.F., Liu, K.B., 1995. Late-glacial stage and Holocene tropical ice core records from Huascarán, Peru. *Science* 269 (5220), 46-50.
- Vera, C., Higgins, W., Amador, J., Ambrizzi, T., Garreaud, R., Gochis, D., Gutzler, D., Lettenmaier, D., Marengo, J., Mechoso, C.R., Nogues-Paegle, J., Silva Dias, P.L., Zhang, C., 2006. Toward a unified view of the American Monsoon Systems. *Journal of Climate* 19 (20), 4977-5000.
- Vuille, M., Werner, M., 2005. Stable isotopes in precipitation recording South American summer monsoon and ENSO variability: observations and model results. *Climate Dynamics* 25, 401-413.
- Yoon, J.-H., Zeng, N., 2010. An Atlantic influence on Amazon rainfall. *Climate Dynamics* 34 (2-3), 249-264.
- Zhou, J.Y., Lau, K.-M., 1998. Does a monsoon climate exist over South America? *Journal of Climate* 11 (5), 1020-1040.
- Zhou, J.Y., Lau, K.-M., 2001. Principal modes of interannual and decadal variability of summer rainfall over South America. *Int. J. Climatol.* 21, 1623-1644.

Lab No.	Type	Core taken from	Depth in cm (relative to piston core)	$\delta^{13}\text{C}$	FMC	^{14}C age \pm error	^{210}Pb age \pm uncorrelated 1s error	Notes
AA87339	^{14}C			-13	1.0160 \pm 0.0120	post-bomb		Terrestrial Plant
AA87340	^{14}C			-16.7	1.0330 \pm 0.0110	post-bomb		Aquatic Plant
Univ. Florida	^{210}Pb	Gravity	0.7				5.68 \pm 3.00	
Univ. Florida	^{210}Pb	Gravity	2.1				13.25 \pm 3.46	
Univ. Florida	^{210}Pb	Gravity	3.4				24.17 \pm 4.43	
Univ. Florida	^{210}Pb	Gravity	4.7				37.47 \pm 6.19	
Univ. Florida	^{210}Pb	Gravity	6.0				40.72 \pm 6.57	
Univ. Florida	^{210}Pb	Gravity	7.2				42.65 \pm 6.72	
Univ. Florida	^{210}Pb	Gravity	8.4				42.66 \pm 6.52	
Univ. Florida	^{210}Pb	Gravity	9.5				47.23 \pm 7.16	
Univ. Florida	^{210}Pb	Gravity	10.6				57.45 \pm 9.26	
Univ. Florida	^{210}Pb	Gravity	11.6				73.12 \pm 13.87	
Univ. Florida	^{210}Pb	Gravity	12.6				105.77 \pm 33.74	
AA91738	^{14}C	Piston	18.8	-30.0	0.9841 \pm 0.0051	129 \pm 42		Macrophyte?
AA87342	^{14}C	Gravity	27.5	-31.3	0.9741 \pm 0.0042	211 \pm 34		Leaf
AA89042	^{14}C	Gravity	46.4	-26.6	0.9430 \pm 0.0150	470 \pm 130		Leaf/insect; Excluded (outlier/too old)
AA87343	^{14}C	Gravity	55.5	-28.4	0.8840 \pm 0.0130	990 \pm 120		Leaf; Excluded (<100 μgC)
AA91739	^{14}C	Piston	61.7	-28.3	0.9820 \pm 0.0051	146 \pm 42		Wood
AA87344	^{14}C	Gravity	65.3	-27.6	0.9808 \pm 0.0077	156 \pm 63		Leaf
AA89040	^{14}C	Gravity	80.2	-27.4	0.9742 \pm 0.0040	210 \pm 33		Leaf
AA91735	^{14}C	Piston	82.2	-26.7	0.9650 \pm 0.0053	286 \pm 44		Wood
AA89044	^{14}C	Gravity	84.1	-28.4	0.9281 \pm 0.0041	600 \pm 35		Bulk Sediment; Excluded (sediment too old)
AA89043	^{14}C	Gravity	94.0	-25	0.9075 \pm 0.0053	780 \pm 46		Bulk Sediment; Excluded (sediment too old)
AA89041	^{14}C	Gravity	106.6	-28.9	0.9550 \pm 0.0130	370 \pm 110		Grass
AA89045	^{14}C	Gravity	107.5	-30.2	0.8939 \pm 0.0039	901 \pm 36		Bulk Sediment; Excluded (sediment too old)
AA91734	^{14}C	Piston	107.9	-16.5	0.9076 \pm 0.0049	778 \pm 43		Macrophyte
AA89046	^{14}C	Gravity	110.3	-27.9	0.9380 \pm 0.0150	520 \pm 130		Grass
AA87341	^{14}C	Gravity	117.9	-21.6	0.7700 \pm 0.0170	2100 \pm 180		Arthropod (probably aquatic); Excluded (<100 μgC)
AA91736	^{14}C	Piston	179.6	-25.2	0.9281 \pm 0.0052	599 \pm 45		Wood/leaf
AA91740	^{14}C	Piston	192.2	-27.9	0.8929 \pm 0.0048	910 \pm 44		Wood
AA91743	^{14}C	Piston	236.7	-26.2	0.8483 \pm 0.0048	1322 \pm 45		Leaf; Excluded (outlier/too old)
AA91741	^{14}C	Piston	260.3	-29.2	0.8639 \pm 0.0045	1175 \pm 42		Seed
AA91745	^{14}C	Piston	312.5	-10.6	0.8424 \pm 0.0051	1378 \pm 48		Wood
AA91744	^{14}C	Piston	349.5	-28.9	0.8375 \pm 0.0046	1424 \pm 44		Macrophyte?
AA91748	^{14}C	Piston	388.0	-27.3	0.8448 \pm 0.0046	1355 \pm 44		Macrophyte or leaf?
AA91746	^{14}C	Piston	426.8	-26.5	0.8330 \pm 0.0060	1467 \pm 58		Macrophyte
AA91747	^{14}C	Piston	467.9	-26.7	0.7861 \pm 0.0060	1933 \pm 61		Excluded (<100 μgC)

Table 1. Lake Limón age model data, including radiocarbon and ^{210}Pb ages.

	PC1	PC2
NATL ERSST	-0.63 (9)	-0.12 (6)
NINO3.4	-0.05 (17)	0.4 (14)
Reuter et al.	0.29 (11)	0.3 (13)
Gray et al.	-0.36 (22)	0.36 (16)
Black et al.	0.26 (9)	-0.17 (12)
Haug et al.	0.5 (23)	0.02 (19)

Table 2. Correlation coefficients for Limón PC1, PC2 and the NATL ERSST, Niño 3.4, Reuter et al., Gray et al., Black et al., and Haug et al. records. ERSST and ENSO indices, 1854-1972 (5 year running means). Reuter et al. (1088-1972), Gray et al. (1567-1972), Black et al. (1221-1972), and Haug et al. (564-1839), 15 year bins. Correlation coefficients at the 95% confidence interval are shown in bold italics and coefficients at the 90% confidence interval are shown in bold. Effective sample sizes (shown in parentheses) were used to account for autocorrelation.

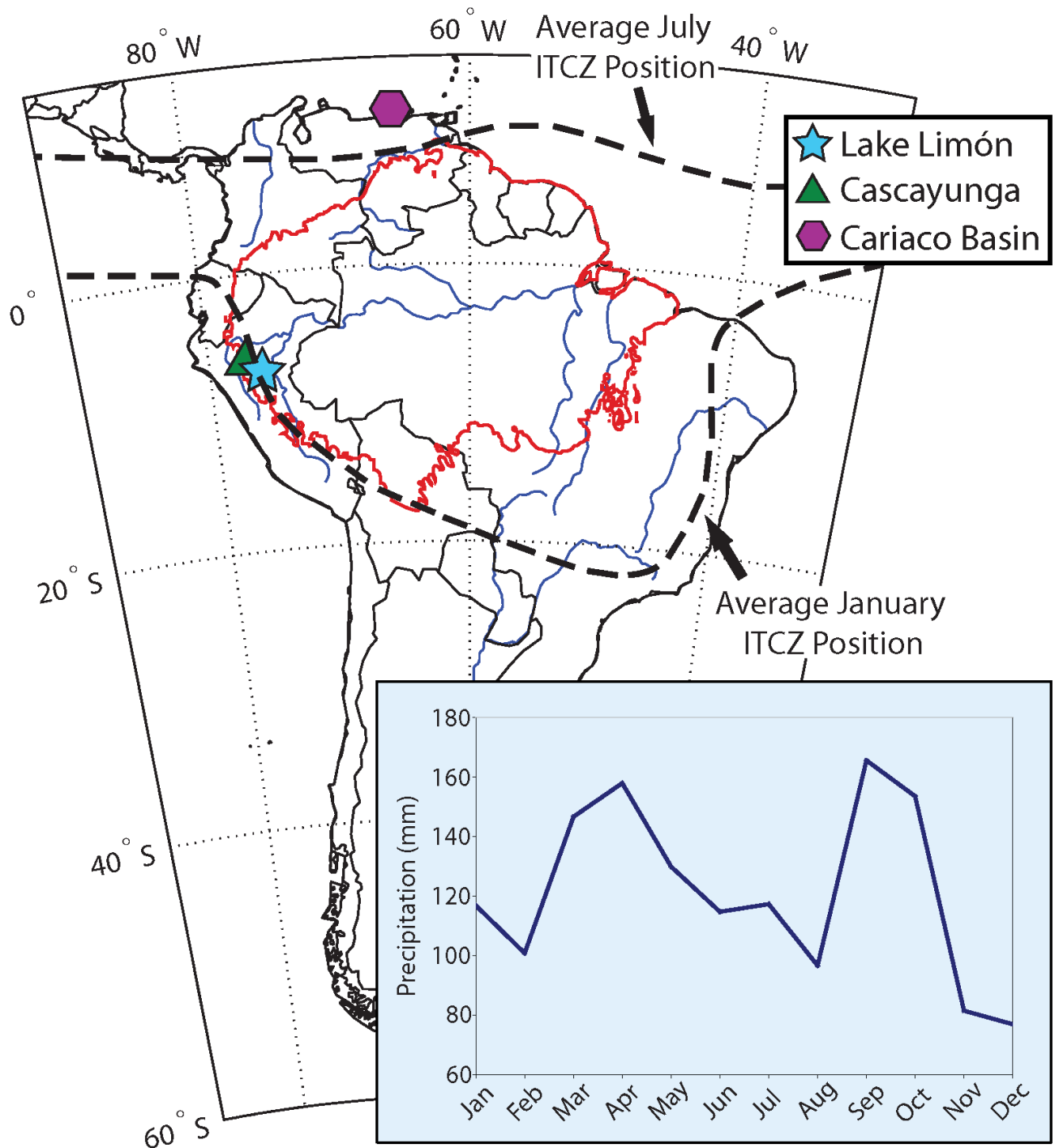


Fig. 1. Map of South America and monthly precipitation for Saucé (closest station to Lake Limón), 1964-1977. Red line is outline of the Amazon Basin. ITCZ position from *Mayle et al.*, [2000].

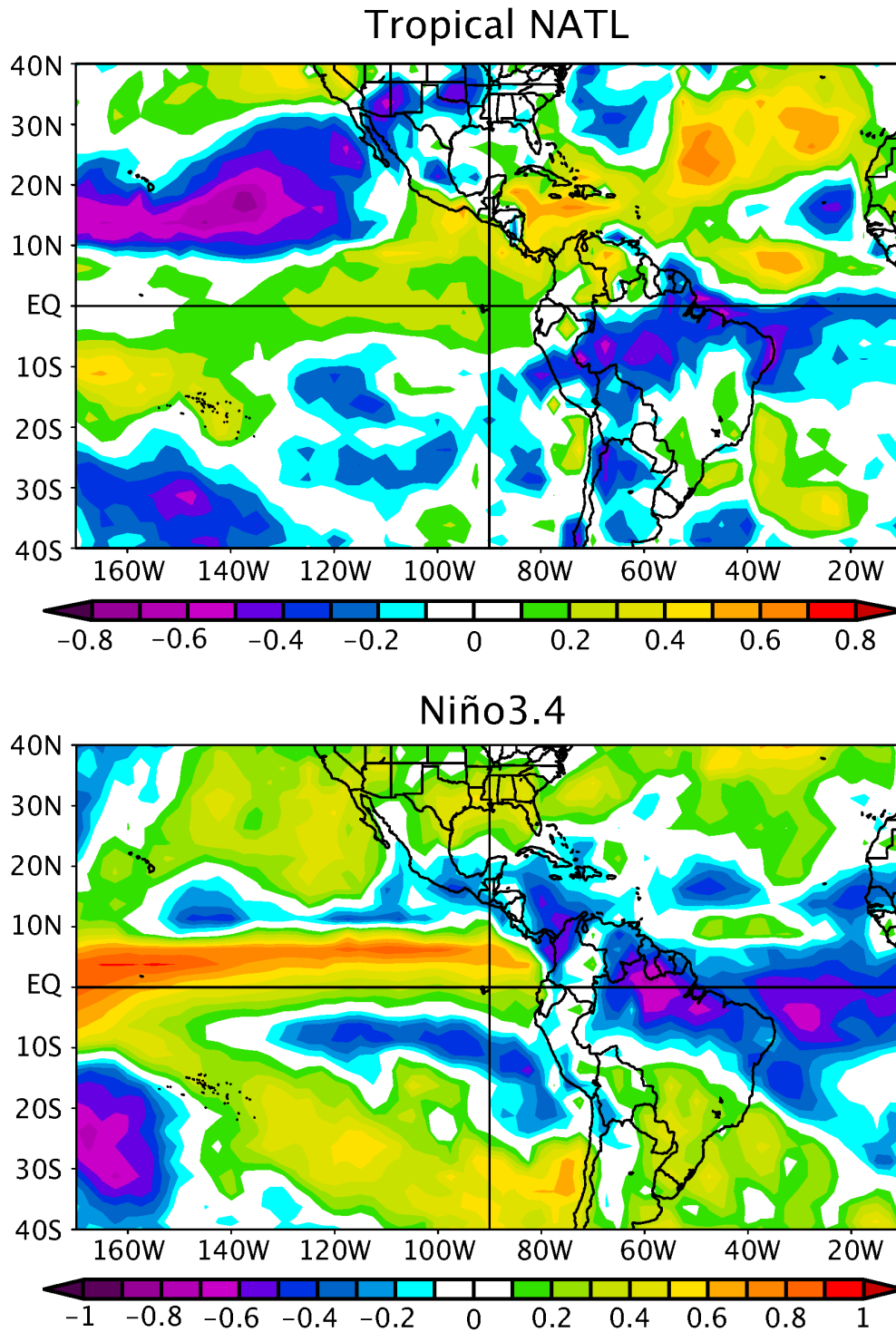


Fig. 2. Correlations between instrumental records of annual 1000mb precipitation (from the GPCP v2.1 data set) [Adler *et al.*, 2003] and tropical NATL SST anomalies (from the GISST and NOAA O1 1x1 data sets, shown in panel A, for the region 5.5°N to 23.5°N, 15°W to 57.5°W) [Enfield *et al.*, 1999] and Niño 3.4 SST (from the CPC data set, shown in panel B) for the period 1979-2007. All data provided by, and correlations computed using the NOAA/OAR/ESRL PSD in Boulder Colorado at their website (<http://www.esrl.noaa.gov/psd/>).

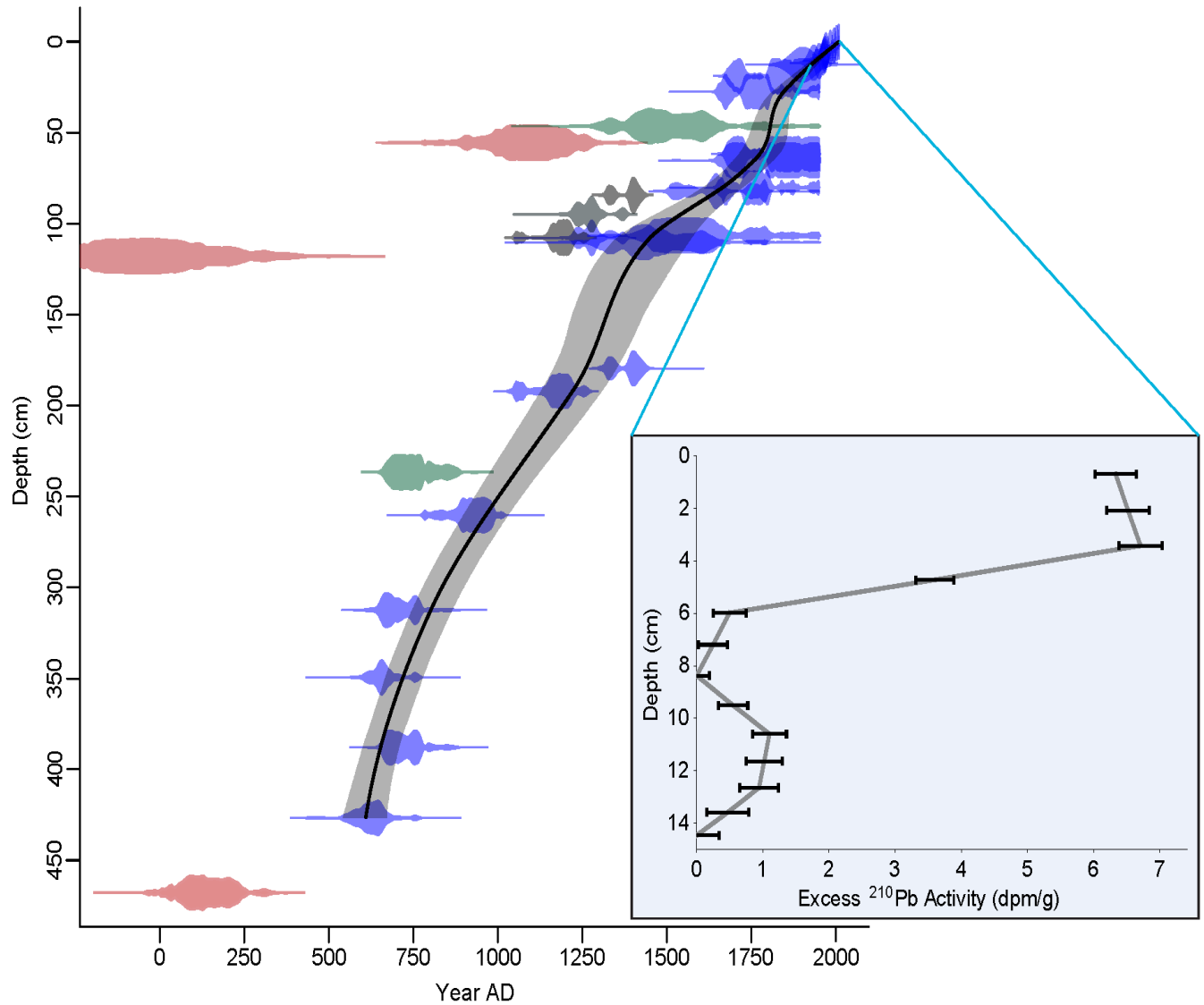


Fig. 3. Limón age model, including radiocarbon and ²¹⁰Pb ages. “Best fit” age model produced in *clam* with a 2 sigma age envelope [Blaauw, 2010]. Dates in purple were used to create the final age model. Dates in pink were excluded due to small size. Dates in green were considered outliers and thus excluded. Dates in dark gray were taken on bulk sediment and were thus excluded. Inset shows unsupported ²¹⁰Pb activity with 1 sigma error bars.

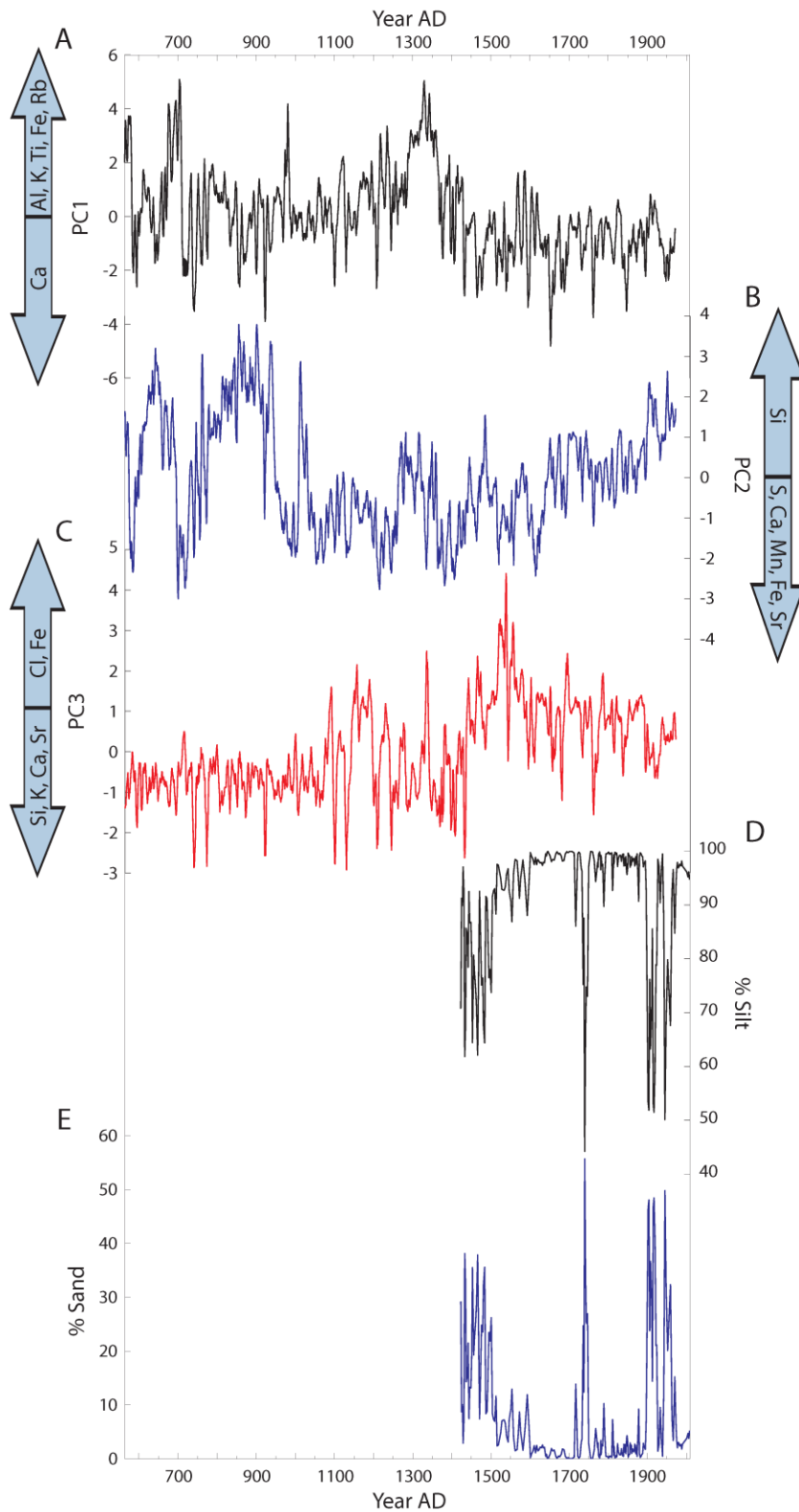


Fig. 4. Limón XRF principal components and grain size values. XRF data shown as 5-year moving averages, 564 to 1972 AD. Grain size values shown as volume percent silt and sand, 564-2008. (A) PC1. (B) PC2. (C) PC3. (D) Percent silt. (E) Percent sand.

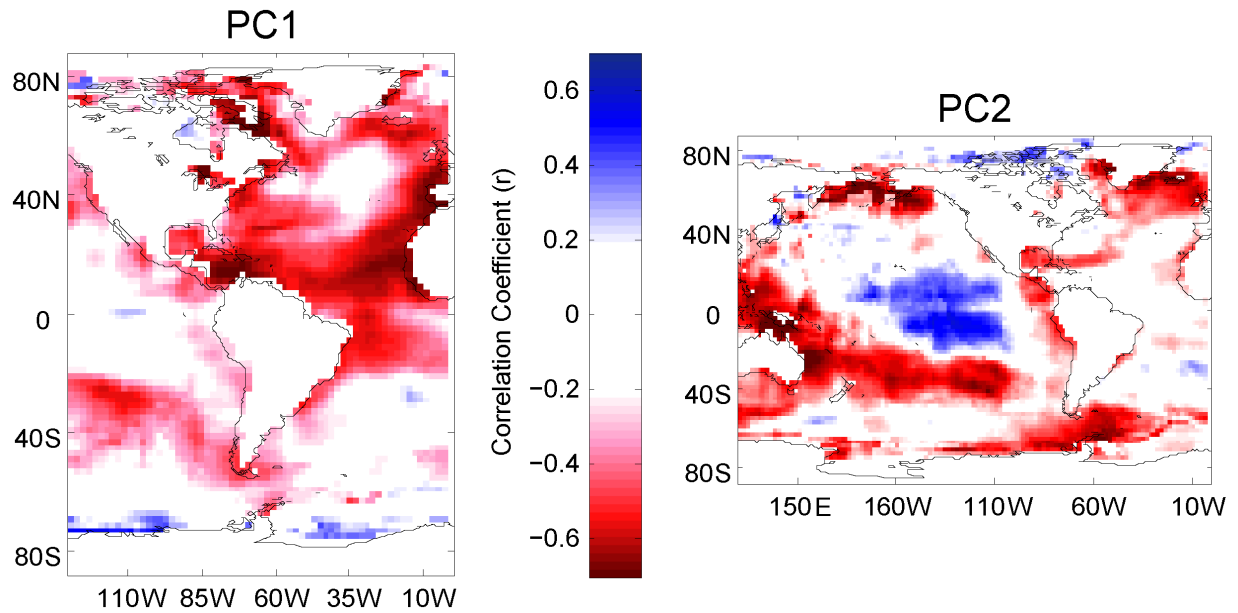


Fig. 5. Maps showing the spatial correlation coefficients between SST (from the ERSST v3b data set) and Limón PC1 (panel A) and PC2 (panel B) for the period 1854-1972 (5 year running means). Warm colors indicate negative correlations, and cool colors indicate positive correlations. Correlations are statistically significant at the 90% confidence interval and were computed with the KMNI Climate Explorer.

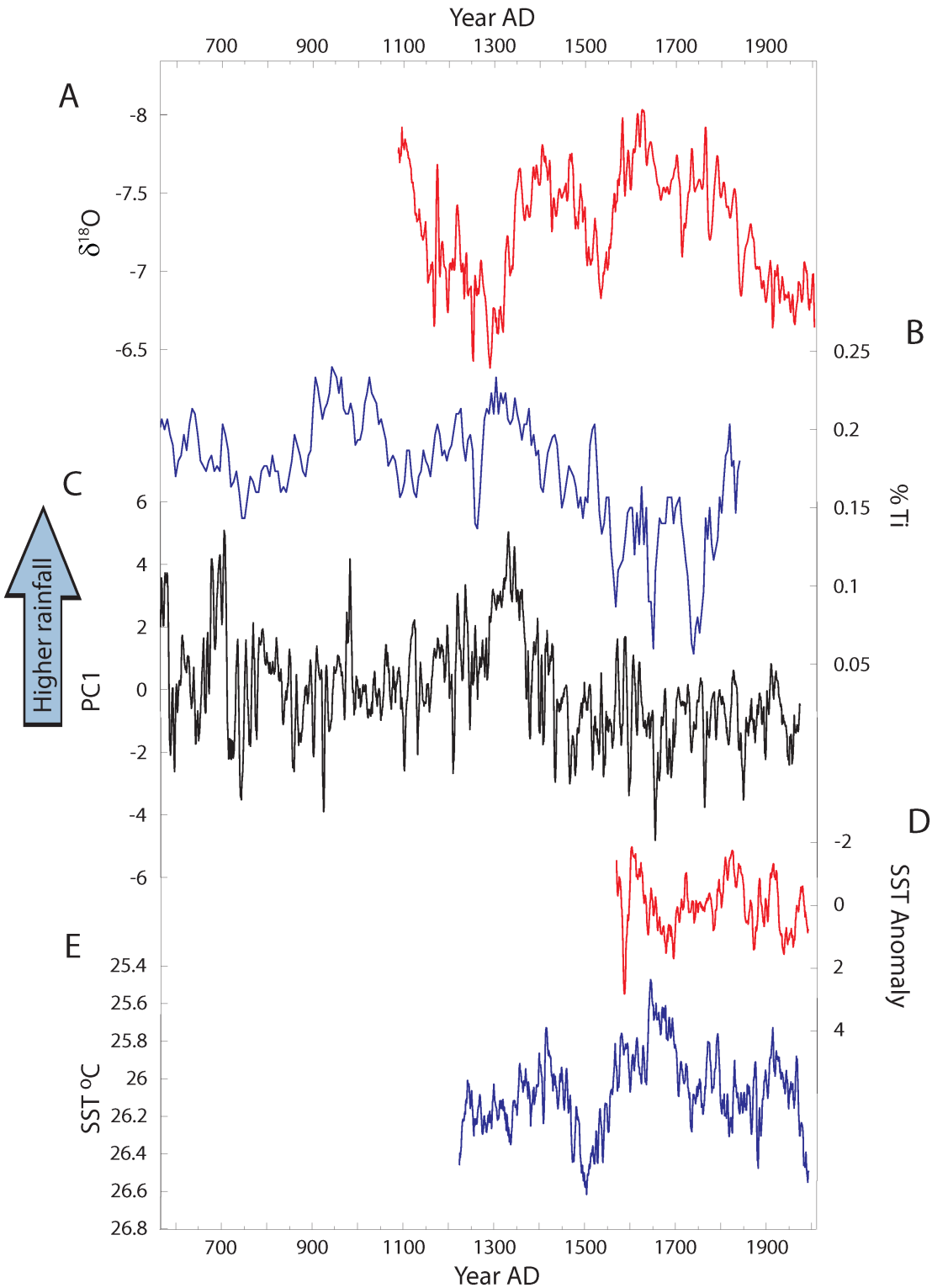
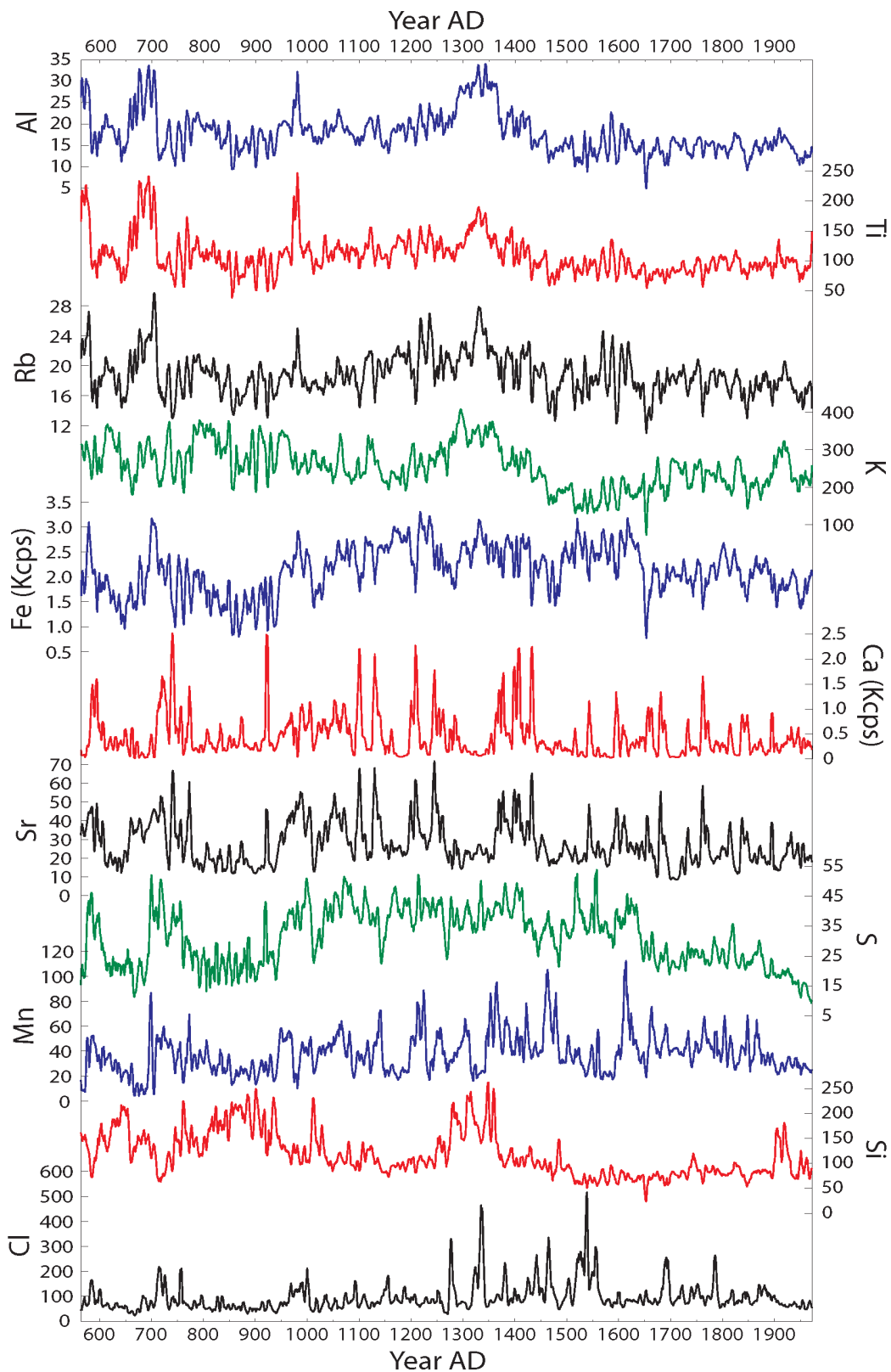


Fig. 6. Limón PC1 with climate reconstructions. (A) Cascayunga speleothem rainfall $\delta^{18}\text{O}$ [Reuter *et al.*, 2009]. (B) Cariaco Basin %Ti Record [Haug *et al.*, 2001]. (C) Limón PC1. (D) NATL SST tree-ring reconstruction [Gray *et al.* 2004]. (E) Cariaco Basin SST [Black *et al.*, 2001]. All data shown as 5-year moving averages. Note reversed axes on panels A, D, and E.



Appendix A: XRF data. All data given in counts per second (cps) except for the elements labeled as thousands of counts per second (Kcps). All data shown as 5-year moving averages.

Element	PC1(38%)	PC2(24%)	PC3(17%)
Al	0.47	-0.09	-0.21
Si	0.20	0.37	-0.32
S	0.07	-0.51	0.04
Cl	-0.09	-0.22	0.40
K	0.36	0.11	-0.34
Ca	-0.28	-0.29	-0.50
Ti	0.44	-0.10	-0.08
Mn	-0.08	-0.34	-0.07
Fe	0.31	-0.39	0.30
Rb	0.47	-0.10	0.12
Sr	-0.13	-0.41	-0.46

Appendix B: Elemental loadings on each principal component. Variance explained by each principal component shown in parentheses.